

Exploring Novel Cd(II) Complexes with 5-Methyl-4-Imidazolecarboxaldehyde: Synthesis, Structure, Computational Insights, and Affinity to DNA through switchSense Methodology

Mateusz Kowalik,^{1,*} Paulina Nowicka,¹ Jakub Brzeski,¹ Natalia Żukowska,¹ Joanna Masternak,² Katarzyna Kazimierczuk,³ Mariusz Makowski¹

¹ Faculty of Chemistry, University of Gdańsk, 80-308 Gdańsk, Poland

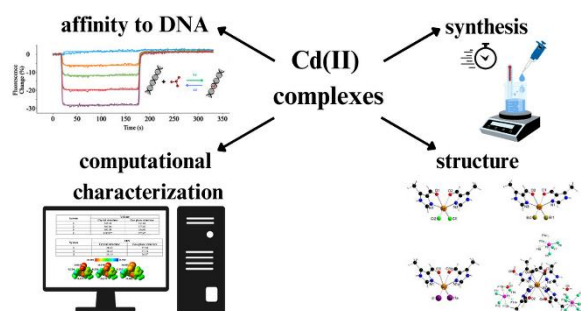
² Institute of Chemistry, Jan Kochanowski University in Kielce, 25-406 Kielce, Poland

³ Faculty of Chemistry, Gdańsk University of Technology, 80-233 Gdańsk, Poland

*Corresponding author: mateusz.kowalik@ug.edu.pl

Keywords: Cd(II), imidazolecarboxaldehyde, crystal structure, computational analysis, switchSense technique

TOC



SYNOPSIS

The study of four Cd(II) complexes with 5-methyl-4-imidazolecarboxaldehyde and different inorganic anions within (Cl^- , Br^- , I^-) or outside (PF_6^-) the coordination sphere using experimental and computational methods including interaction with DNA using the innovative switchSense technique were carried out.

Abstract

A series of four Cd(II) complexes with 5-methyl-4-imidazolecarboxaldehyde (**L**) with different inorganic anions within or outside the coordination sphere of general formula: [CdCl₂L₂] (**1**), [CdBr₂L₂] (**2**), [CdI₂L₂] (**3**), and [CdL₄](PF₆)₂·3H₂O (**4**) was synthesized through one-step and two-step reactions, respectively. All complexes were obtained as colorless crystals without the need for recrystallization and exhibited solubility in aqueous solutions. Structural analysis revealed different coordination environments for each complex, with variations in bond lengths and angles. The crystal packing of the complexes was stabilized by hydrogen bonding and π - π stacking interactions. FT-IR analysis indicated coordination of the ligand to the metal ion, and UV-Vis studies confirmed the stability of the complexes in solution. Computational analysis has revealed the polar nature of the complexes and their favorable stability constants. Affinity studies with DNA using the switchSense technique demonstrated rapid association and dissociation processes for all complexes, with temperature-dependent binding constants. Thermodynamic analysis suggested spontaneous with positive entropy change and endothermic formation processes for the complexes. Overall, the study underscores the synthesis, examination, and interaction with DNA of Cd(II) complexes, demonstrating their promise within medicinal chemistry.



Introduction

Cadmium is a toxic non-essential transition metal that poses a health risk for both humans and animals, and it is naturally occurring in the environment as a pollutant that is derived from agricultural and industrial activities [1]. Therefore, understanding the coordination chemistry of Cd(II) complexes is important for developing strategies to mitigate the harmful effects of cadmium exposure. However, as a transition metal of Group 12 of the periodic table exhibits the ability to form coordination complexes with various ligands. These complexes can be studied for their structural, physicochemical, and biological properties with the use of both traditional experiments and computational methods. There are several methods to study Cd(II) complexes, including spectroscopic techniques, elemental analysis, X-ray single-crystal diffraction [2], computational methods [3], and polarographic studies [4]. These methods can provide insights into the coordination chemistry of Cd(II) complexes and their possible applications.

Cd(II) forms a variety of complexes with different ligands, leading to diverse structural and chemical properties. Some examples of Cd(II) complexes include those incorporating di-2-pyridylmethanone N-(2-pyridinyl)hydrazone (DPMNPH) [5], (arylo)imidazoles [6], cysteine, penicillamine [4], 3-hydrazino-4-amino-1,2,4-triazole [7], and 2,6-bis(3,4,5-trimethylpyrazolyl)pyridine (btmpp) [8]. These complexes [4, 6–8] exhibit various nuclearities, dimensionalities, and coordination geometries and also potential applications, such as in the field of anti-proliferative activity [8]. A compelling study on Cd(II) complexes was performed by Barszcz et al. [9]. The study reports a comparative investigation of the coordination chemistry of calcium and cadmium model complexes. Cd(II) and Ca(II) complexes with N,O-bidentate ligands derived from pyridine and imidazole were synthesized and characterized. Cd(II) complex with 5-methyl-4-imidazolecarboxaldehyde and NO_3^- anions showed the most potent antitumor activity in leukemia and cervical carcinoma. Finally, it offers an understanding of the chemical properties of Cd(II) complexes and their possible uses.

The biological properties of Cd(II) complexes have been also a subject of research, with findings indicating biomedical applications. For instance, a study reported the design of two new Cd(II) complexes as bio-active materials, which were characterized using various spectroscopic techniques and X-ray single-crystal diffraction [2]. Another study focused on the cytotoxic properties of Cd(II) complexes, revealing their effectiveness as anticancer agents with a wide spectrum of action and a beneficial pharmacological profile [10]. Additionally, the



sensitivity of neuroblastoma cells to Cd(II) complexes was investigated, with promising results indicating the inhibition of cell growth [10].

The stereochemistry of Cd(II) complexes with ligands in biological fluids is also an area of interest for understanding their interactions with biomolecules. Studies have focused on the design of Cd(II) complexes as bio-active materials, their cytotoxic properties, and their coordination with specific ligands such as cysteine and penicillamine [2, 4, 11]. Research has shown that Cd(II) complexes exhibit cytotoxic properties, making them candidates for anticancer agents with a wide spectrum of action.

The toxicity of Cd(II) is comparable to that of noble metals such as Pt and Pd, which have found medical applications. It has been shown that the toxicity of a metal cannot be considered a constant property because it depends on many factors, including the type of ligand presented in the complex [12]. Coordination connections with metal ions may demonstrate a more effective mechanism of action than free ligands [13]. One of the most famous examples of a drug based on a coordinatively bonded metal ion is cisplatin, used in anticancer therapy. Therefore, the search for new potential pharmaceuticals often focuses on designing coordination compounds that would contain another central atom from transition metals. There are more and more reports in the literature about the biological activity of Cd(II) complexes. It has been shown that some of them directly target the DNA chain and inhibit of incorporation of 3H-thymidine into DNA [14]. Furthermore, they can target DNA non-covalently by groove binding [15], intercalation [16–18], or combinations of these two modes [19]. In addition to DNA, they can also be directed at other protein targets [20–23]. In the case of cancer cells, they inhibit their respiration and also lead to their death through apoptosis [14, 20–22, 24]. Apart from this, Cd(II) coordination compounds may have stronger antimicrobial activity than some previously used antibiotics [25–27]. Consequently, they constitute an important group of connections in the search for new biologically active compounds.

The nature of ligands greatly influences the properties of Cd(II) complexes toward lowering their toxicity. Imidazolecarboxaldehyde and its derivatives as ligands contribute to the unique characteristics of the resulting complexes. The choice of ligands not only affects the stability and structure of the complexes but also plays a crucial role in determining their reactivity and applications. One of the most promising ways of exploration is the study of Cd(II) complexes with imidazolecarboxaldehyde as a ligand. Imidazolecarboxaldehyde and its derivatives have been studied for their various biological properties, including antimicrobial, antioxidant, and



anti-inflammatory activities. Imidazole derivatives, including Schiff bases and transition metal complexes, have shown antimicrobial and antioxidant properties [28–33].

Our ongoing research presents the study of four Cd(II) complexes with 5-methyl-4-imidazolecarboxaldehyde (**L**) with different inorganic anions within or outside the coordination sphere. Four complexes [CdCl₂L₂] (**1**), [CdBr₂L₂] (**2**), [CdI₂L₂] (**3**), and [CdL₄](PF₆)₂·3H₂O (**4**) were synthesized and characterized in detail by elemental analysis, mass spectrometry, and FT-IR spectroscopy. The structures of crystals were solved using SC-XRD analysis. The experimental results were then compared with theoretical calculations [2, 34] on stability, dipole moments, Molecular Electrostatic Potential (MEPS), molecular volume, and polarity. Compounds were studied toward their stability in solution with the use of UV-Vis, and interaction with DNA using the switchSense technique [35, 36].

Experimental

Materials and physicochemical measurements

All commercial reagents were used as supplied without further purification. The Cd(II) chloride and acetate as well as potassium bromide and iodide were purchased from POCH S.A., while ammonium hexafluorophosphate and 4-methyl-5-imidazolecarboxaldehyde from Sigma-Aldrich.

Elemental analysis for carbon, hydrogen, and nitrogen was performed on an Elementar Vario El Cube CHNS analyzer (Elementar). Mass spectra were obtained using a Bruker Daltonics (HCT Ultra) instrument. The infrared spectra were recorded on a Perkin Elmer Spectrum Two FT-IR spectrometer using an attenuated total reflectance (ATR) module with a diamond crystal in the spectral range of 4000–400 cm⁻¹. The intensity of FT-IR bands was indicated as: s (strong), m (medium), and w (weak).

Stability studies in solution of ligand (**L**) and Cd(II) complexes ([**L**] = 1·10⁻⁴ M, [**1–4**] = 1·10⁻⁵ M) were carried out in TE40 buffer (used in SwitchSense technique) by UV-Vis spectrophotometry using a Jasco V-630 spectrophotometer. Spectra in the range 215–700 nm were recorded at room temperature immediately after dissolution (0 h), after 24 and 48 hours.

Synthesis

Complex 1

The aqueous solution (10 cm³) containing 1.0 mmol (110.1 mg) of 5-methyl-4-imidazolecarboxaldehyde (L) was mixed with aqueous solution (5 cm³) of 0.5 mmol (114.2 mg) Cd(II) chloride and stirred at 70 °C for 3 hours. The molar ratio of CdCl₂:L was 1:2. After one week colourless crystals were obtained and air dried.

Complexes 2–4

To the mixture of 0.5 mmol (133.3 mg) Cd(II) acetate and 1.0 mmol (110.1 mg) 5-methyl-4-imidazolecarboxaldehyde in water (15 cm³), an aqueous solution (5 cm³) of appropriate salt (2.0 mmol) was added dropwise: potassium bromide (238.0 mg) for **2**, potassium iodide (332.0 mg) for **3** and ammonium hexafluorophosphate (326.0 mg) for **4**. The molar ratio of (CH₃COO)₂Cd:L:KBr/KI/NH₄PF₆ was 1:2:4. The clear solutions were stirred for 3 hours at 70 °C. A few days later colourless crystals were collected and air dried.

[CdCl₂L₂] (1)

Yield: 78%. Anal. Calc. (%) for C₁₀H₁₂CdCl₂N₄O₂: C, 29.76; H, 3.00; N, 13.88. Found (%): C, 29.87; H, 3.01; N, 13.79. FT-IR ATR (cm⁻¹): 3119 (m), 3013 (m), 2949 (w), 2892 (w), 1765 (w), 1642 (s), 1616 (s), 1589 (s), 1516 (m), 1436 (s), 1398 (w), 1356 (s), 1311 (s), 1243 (s), 1143 (m), 971 (s), 877 (m), 832 (m), 810 (s), 685 (m), 637 (s), 549 (w). ESI-MS (CH₃OH/H₂O, *m/z* exp./theor.): 365.0–371.0/368.1 [M–Cl]⁺, 329.0–335.0/331.7 [M–2Cl–H]⁺, 254.8–260.8/258.0 [M–L–Cl]⁺.

[CdBr₂L₂] (2)

Yield: 81%. Anal. Calc. (%) for C₁₀H₁₂CdBr₂N₄O₂: C, 24.39; H, 2.46; N, 11.38. Found (%): C, 24.43; H, 2.40; N, 11.32. FT-IR ATR (cm⁻¹): 3163 (m), 3117 (m), 2898 (w), 1752 (w), 1659 (s), 1619 (s), 1590 (s), 1512 (m), 1431 (s), 1397 (w), 1375 (m), 1355 (s), 1308 (m), 1242 (s), 1145 (m), 1102 (m), 1034 (w), 969 (s), 810 (s), 782 (s), 695 (s), 682 (s), 634 (s), 562 (m), 546 (m). ESI-MS (CH₃OH/H₂O, *m/z* exp./theor.): 409.0–414.9/412.5 [M–Br]⁺, 329.0–335.0/331.7 [M–2Br–H]⁺, 298.9–304.9/302.4 [M–L–Br]⁺.

[CdI₂L₂] (3)

Yield: 70%. Anal. Calc. (%) for C₁₀H₁₂CdI₂N₄O₂: C, 20.48; H, 2.06; N, 9.55. Found (%): C, 20.46; H, 2.07; N, 9.36. FT-IR ATR (cm⁻¹): 3122 (w), 3017 (w), 2951 (w), 2899 (w), 1622 (s),



1588 (m), 1519 (m), 1449 (s), 1399 (w), 1359 (s), 1317 (m), 1249 (m), 1149 (m), 1098 (w), 973 (s), 817 (s), 683 (m), 638 (s), 564 (m), 552 (m). ESI-MS (CH₃OH/H₂O, *m/z* exp./theor.): 456.9–462.9/459.5 [M–I]⁺, 346.9–352.9/349.4 [M–L–I]⁺, 329.0–335.0/331.7 [M–2I–H]⁺.

[CdL₄](PF₆)₂·3H₂O (**4**)

Yield: 58%. Anal. Calc. (%) for C₂₀H₃₀CdF₁₂N₈O₇P₂: C, 26.78; H, 3.37; N, 12.49. Found (%): C, 26.71; H, 3.26; N, 12.71. FT-IR ATR (cm⁻¹): 3653 (w), 3146 (w), 3088 (w), 3020 (w), 2900 (w), 1650 (s), 1623 (s), 1523 (m), 1451 (m), 1399 (w), 1360 (s), 1318 (m), 1258 (m), 1150 (w), 1111 (w), 973 (m), 830 (s), 814 (s), 741 (m), 684 (m), 640 (s), 556 (s). ESI-MS (CH₃OH/H₂O, *m/z* exp./theor.): 349.0–355.0/353.6 [M–3H₂O–2PF₆–2L–2H+Na]⁺, 329.0–335.0/331.7 [M–3H₂O–2PF₆–2L–H]⁺, 238.8–244.9/243.5 [M–3H₂O–2PF₆–3L–2H+Na]⁺.

Crystal structure determination and refinement

The X-ray diffraction data were collected on an IPDS 2T dual-beam diffractometer at 120.0(2) K with Mo K α radiation of a microfocus X-ray source (GeniX 3D Mo HighFlux, 50 kV, 1.0 mA, $\lambda = 0.71069$ Å) for the structures. Every crystal was thermostated in a nitrogen stream at 120 K using a CryoStream-800 device during the entire experiment. The X-Area 1.75 program controlled data collection and data reduction [37]. The structure was solved by the SHELXT method [38] and refined using the program packages Olex2 [39] and SHELX-2015 [40]. Diamond [41] was used to prepare the figures. All non-hydrogen atoms were modeled as anisotropic, and H atoms were refined as isotropic. Hydrogen atoms were placed in idealized positions and refined with the usual restraints of the riding model. Two structures were refined as a two component twin with the domain's mass fraction equal to 0.26487 for **1** and 0.03892 for **3**, using HKLF5 instruction under SHELXL. The fluorine atoms of the hexafluorophosphate ions in **4** needed to be modelled as disordered: F1–F5 (s.o.f. of 0.508(13) and 0.492(13)) and F7 (s.o.f. of 0.772(13) and 0.228(13)). The crystallographic data and some details of the structural refinement are summarized in Table 1.

Crystallographic data for all structures reported in this paper have been deposited with the Cambridge Crystallographic Data Centre as supplementary publication no. CCDC 2311088–2311091. The data can be obtained free of charge from The Cambridge Crystallographic Data Centre via <http://www.ccdc.cam.ac.uk/structures>.



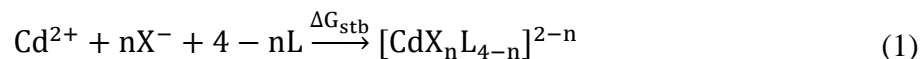
Table 1.
Crystallographic data and structure refinement details for complexes **1–4**.

Compound reference	1 (CCDC-2311088)	2 (CCDC-2311089)	3 (CCDC-2311090)	4 (CCDC-2311091)
Empirical formula	C ₁₀ H ₁₂ CdCl ₂ N ₄ O ₂	C ₁₀ H ₁₂ Br ₂ CdN ₄ O ₂	C ₁₀ H ₁₂ Cd I ₂ N ₄ O ₂	C ₂₀ H _{28.62} CdF ₁₂ N ₈ O _{6.3} P ₂
<i>M_r</i> / g mol ⁻¹	403.55	492.46	586.44	884.45
Temperature /K	120(2)	120(2)	120(2)	120(2)
Wavelength /Å	0.71073 (Mo K _α)			
Crystal system	triclinic	monoclinic	monoclinic	tetragonal
Space group	$\bar{P}1$	<i>P</i> 2 ₁ / <i>c</i>	<i>C</i> 2/ <i>c</i>	<i>I</i> 4 ₁ / <i>a</i>
<i>a</i> /Å	7.132(3)	7.1894(6)	18.2229(18)	26.8364(12)
<i>b</i> /Å	8.627(4)	7.6975(9)	7.8751(6)	26.8364(12)
<i>c</i> /Å	12.649(6)	26.177(3)	15.1100(15)	19.1349(9)
α /°	69.79(4)	90	90	90
β /°	75.84(4)	97.113(8)	130.501(6)	90
γ /°	78.74(4)	90	90	90
<i>V</i> /Å ³	702.9(6)	1437.5(3)	1648.8(3)	13780.8(14)
<i>Z</i>	2	4	4	16
Calculated density /Mg m ⁻³	1.907	2.276	2.362	1.705
μ /mm ⁻¹	1.935	7.081	5.072	0.839
<i>F</i> (000)	396	936	1080	7058
θ range /°	2.535 to 26.499	2.760 to 29.248	2.770 to 29.215	2.146 to 25.999
Limiting indices	-8 ≤ <i>h</i> ≤ 8 -9 ≤ <i>k</i> ≤ 10 -15 ≤ <i>l</i> ≤ 15	-9 ≤ <i>h</i> ≤ 9 -10 ≤ <i>k</i> ≤ 10 -35 ≤ <i>l</i> ≤ 35	-24 ≤ <i>h</i> ≤ 24 -10 ≤ <i>k</i> ≤ 10 -20 ≤ <i>l</i> ≤ 20	-33 ≤ <i>h</i> ≤ 33 -33 ≤ <i>k</i> ≤ 33 -23 ≤ <i>l</i> ≤ 23
Reflections collected / unique	2899 / 2899 [<i>R</i> _{int} = merged]	22967 / 3890 [<i>R</i> _{int} = 0.0462]	9695 / 9695 [<i>R</i> _{int} = merged]	85017 / 6772 [<i>R</i> _{int} = 0.0387]
Completeness to θ_{\max} /%	99.9	100	94.9	99.9
Refinement method	Full-matrix least-squares on <i>F</i> ²			
Data/restraints/parameters	2899 / 0 / 175	3890 / 0 / 174	9695 / 0 / 89	6772 / 66 / 512
Goodness-of-fit on <i>F</i> ²	1.054	1.024	1.096	1.052
Final <i>R</i> indices [<i>I</i> > 2σ(<i>I</i>)]	<i>R</i> ₁ = 0.0561 <i>wR</i> ₂ = 0.1532	<i>R</i> ₁ = 0.0266 <i>wR</i> ₂ = 0.0645	<i>R</i> ₁ = 0.0262 <i>wR</i> ₂ = 0.0695	<i>R</i> ₁ = 0.0467 <i>wR</i> ₂ = 0.1325
<i>R</i> indices (all data)	<i>R</i> ₁ = 0.0649 <i>wR</i> ₂ = 0.1604	<i>R</i> ₁ = 0.0330 <i>wR</i> ₂ = 0.0671	<i>R</i> ₁ = 0.0276 <i>wR</i> ₂ = 0.0704	<i>R</i> ₁ = 0.0531 <i>wR</i> ₂ = 0.1381
Largest diff. peak and hole /eÅ ⁻³	1.608; -1.595	1.048; -0.714	0.590; -0.782	1.903; -1.007

Computational methods

The quantum chemical calculations were conducted in two manners. Namely, both the structures from the X-ray as well as those with geometries optimized computationally were investigated. The single-point calculations on X-ray structures were conducted using the second-order Møller–Plesset perturbation theory [42, 43] together with double- ζ correlation-consistent Dunning type basis set – aug-cc-pVDZ [42, 43] for all atoms but Cd and I. For Cd and I atoms the aug-cc-pVDZ-PP basis set was used [44, 45]. The optimization of crystal structures **1**, **2**, and **3** as well as their vibrational analysis was performed at the same level. Due to the significantly higher size of system **4**, the corresponding gradients as well as the force constants were calculated using cc-pVDZ-PP (for Cd) and cc-pVDZ (for remaining atoms). To

get the comparable results of wave function analyses, the single-point calculation of **4** was carried out at the same aug-cc-pVDZ/aug-cc-pVDZ-PP basis set as for **1**, **2**, and **3**. The thermodynamic stability (ΔG_{stb}) of all coordination compounds was established as Gibbs free energies (at $T = 298.15$ K) associated with corresponding formation reactions:



where X and L symbolize halogen and imidazole's derivative substituent, respectively. For systems **1–3** the stabilities were established using the aug-cc-pVTZ-PP/aug-cc-pVTZ basis set. The thermodynamic stability characterizing **4** was evaluated using the electronic energies of **4** and its ligands obtained using the aug-cc-pVTZ-PP/aug-cc-pVDZ basis set and the zero-point energy corrections, thermal corrections and entropy contributions (at $T = 298.15$ K) estimated using cc-pVTZ-PP/cc-pVDZ basis set. This approach guarantees that the determined thermodynamic stabilities of all **1–4** can be compared. The Cartesian coordinates of all gas-phase structures can be found in Table S1. All quantum chemical calculations were carried out with the use of the GAUSSIAN16 (Revision C.01) computational package [46].

The wave functions containing generalized MP2 densities derived from Z-Vector [47] were then subjected to various analyses conducted using the Multiwfn (Version 3.8) software [48]. The Fuzzy Bond Order (FBO) [49] method is used to characterize the multiplicity of the dative bonds formed. Furthermore, the quantitative analysis of molecular surface was conducted to assess the volume and polarity of studied systems [50]. The FBO between atoms A and B was calculated according to the equation:

$$\text{FBO} = \sum_{\mu, \nu} [(DS^A)_{\mu\nu}(DS^B)_{\nu\mu} + (P^S S^A)_{\mu\nu}(P^S S^B)_{\nu\mu}] \quad (2)$$

where, D and P^S are the matrices of total density and spin density respectively, whereas S is an overlap matrix of basis functions. The volume of studied compounds was assessed using the Marching Tetrahedra method, whereas the polarity was assessed using the so-called Molecular Polarity Index (MPI):

$$\text{MPI} = \frac{1}{A} \iint_S |V(r)| dS \quad (3)$$

where A, $V(r)$, and S describe the area of the van der Waals surface, the value of electrostatic potential, and the molecular surface respectively [51].

SwitchSense kinetics measurement

Materials

The solutions of ligand (**L**) and Cd(II) complexes **1–4** (analytes) were prepared and measured in the same five concentrations: $1.6 \cdot 10^{-3}$, $8.0 \cdot 10^{-4}$, $4.0 \cdot 10^{-4}$, $2.0 \cdot 10^{-4}$ and $1.0 \cdot 10^{-4}$ M. All samples were prepared using the TE40 buffer (pH 7.4; 10 mM Tris-HCl, 40 mM NaCl, 0.05% Tween20, 50 μ M EDTA, 50 μ M EGTA). All solutions necessary for switchSense measurements (TE40 buffer, regeneration, passivation, and standby solutions) and consumables (chip, 96-well plates, and 1.3 and 10.0 mL autosampler vials with caps) were purchased from Dynamic Biosensors GmbH. Double distilled and additionally filtered water was used to prepare buffers and solutions requiring dilution. To reduce the evaporation of samples and the possibility of their contamination during measurement, sealing for 96 well plates was used.

The measuring system

The measurement system consists of a standard available chip (heliX adapter chip with 2 spots). According to the data provided by the gold manufacturer, the chip surface after immobilization contains a fragment of DNA as a ligand with a sequence of 96 base pairs, which contains the lower free strand sequence (5'– ATC AGT ACT TGT CAA CAC GAG CAG CCC GTA TAT TCT CCT ACA GCA CTA –3') and the upper one (5'-48 bases, which are the manufacturer's SECRET + TAG TGC TGT AGG AGA ATA TAC GGG CTG CTC GTG TTG ACA AGT ACT GAT –3'), which is labeled with a fluorophore (red Ra dye). Both spots 1 and 2 are functionalized in the same way. This enables selective and interchangeable functionalization, which allows for multiple regeneration of the chip surface.

Static mode of measurements and result analysis

The experiments were conducted in a static mode using the software and method for weak binder kinetics provided by Dynamic Biosensor, the manufacturer. Functionalization was the initial step in all experiments, with an adapter concentration of $1 \cdot 10^{-7}$ M and a processing time of 200 s. Subsequently, kinetics analysis was performed for five concentration variants, including a blank and the remaining five concentrations as listed. Association and dissociation times were set at 160 s and 150 s, respectively, with a flow rate of $200 \mu\text{L} \cdot \text{s}^{-1}$. Measurements were recorded at five temperatures: 15, 20, 25, 30, and 37 °C. Dissociation continued until complete removal of the analyte by the buffer solution. Blank measurements were conducted before and after each concentration series. To ensure the chips' parameters and conditions were



controlled, a chip test procedure using the manufacturer's method was performed after each series of measurements. The adjustment of the method was described in detail in our previous paper [36]. The results were analyzed using heliOS software (version 2023.4.1). All response curves as fluorescence changed during the ongoing processes (as one data set for the results of five different concentrations) were fitted using an interaction model and then the association/dissociation constants were calculated as previously described in detail [36].

Thermodynamic parameters

To estimate the entropic (ΔS) and energetic (ΔH) contributions to the ΔG , first, we calculated ΔG_i of association process (K_{Ai}) obtained utilizing switchSense at a given temperature (T_i) as expressed by equation 4. The entropic and energetic contributions were then computed concerning the temperature by using a right-difference formula with equal right intervals, as given by equations 5 and 6, respectively [52]:

$$\Delta G_i(T_i) = \ln 10 \cdot RT_i \cdot pK_{Ai}(T_i) \quad (4)$$

$$\Delta S_i(T_i) = -\left(\frac{\partial \Delta G_i(T_i)}{\partial T_i}\right) \quad (5)$$

$$\Delta H_i(\Delta T_i) = \Delta G_i(\Delta T_i) - T_i \Delta S_i(T_i) \quad (6)$$

Then the plots of the parameters from eqs. 4–6 as functions of temperature were plotted.

Results and discussion

Synthesis

Complex **1** was prepared in a one-step reaction between Cd(II) chloride and ligand. While, as a source of Cd(II) ions for the synthesis of complexes **2–4** the Cd(II) acetate was used and mixed with ligand (first step). To the resulting solution, the appropriate salt containing Br^- , I^- and PF_6^- anions was added (second step). All four complexes were isolated directly as air-stable colorless crystals not requiring recrystallization. The compounds proved to be soluble in aqueous solutions such as TE40 buffer used in further studies. In the ESI-MS spectra (Figs. S1–S4) there are observed peaks originating from fragments of Cd(II) complexes such as $[\text{CdXL}_2]^+$, $[\text{CdXL}]^+$, $[\text{CdL}_2\text{-H}]^+$, $[\text{CdL-H}]^+$ and $[\text{CdL}_2\text{-2H+Na}]^+$, where X = Cl (**1**), Br (**2**) or I (**3**).

Description of the structures

The molecular structures of complexes **1–4** are shown in Figure 1, while bond lengths and angles are in Tables S2 and S3, respectively. The complex **1** crystallized in the $P\bar{1}$ space group. The Cd(II) ion is coordinated by two aldehyde molecules bounded in the chelating $\kappa^2\text{N,O}$ fashion. The distorted octahedral coordination environment is completed by two monodentate chloride ligands forming neutral $[\text{CdCl}_2\text{L}_2]$ units (Fig. 1a). Complexes **2** and **3** are composed of similar units $[\text{CdX}_2\text{L}_2]$, where $\text{X} = \text{Br}^-$ for **2** and I^- for **3** (Figs. 1b and 1c, respectively). Complex **2** crystallized in the $P2_1/c$, while complex **3** in the $C2/c$ space group. The observed Cd–N bond distances (2.248–2.312 Å) are in good agreement with the values for similar Cd(II) complexes reported previously. The O-donors formed bonds with more varied lengths from 2.556 Å to 2.718 Å, however, as observed in the literature [53]. Complex **4** crystallized in the tetragonal system, space group $I4_1/a$. The molecular structure is different from others since the Cd(II) ion formed a cationic complex general composition $[\text{CdL}_4]^{2+}$. The charge neutrality is balanced by two PF_6^- ions. There are also water molecules in the crystal lattice of **4** (Fig. 1d). The four organic ligands involved eight donor atoms and formed a distorted dodecahedral polyhedron around the central ion. The Cd(II) coordination environment in **4** can be also described as a double coordination sphere due to the significant variation in the Cd–N and Cd–O bond lengths [54]. The inner coordination sphere consists of four N-donors with shorter bond lengths (2.260–2.307 Å), while the external coordination sphere is composed of four O-donors with longer bond lengths (2.621–2.873 Å).

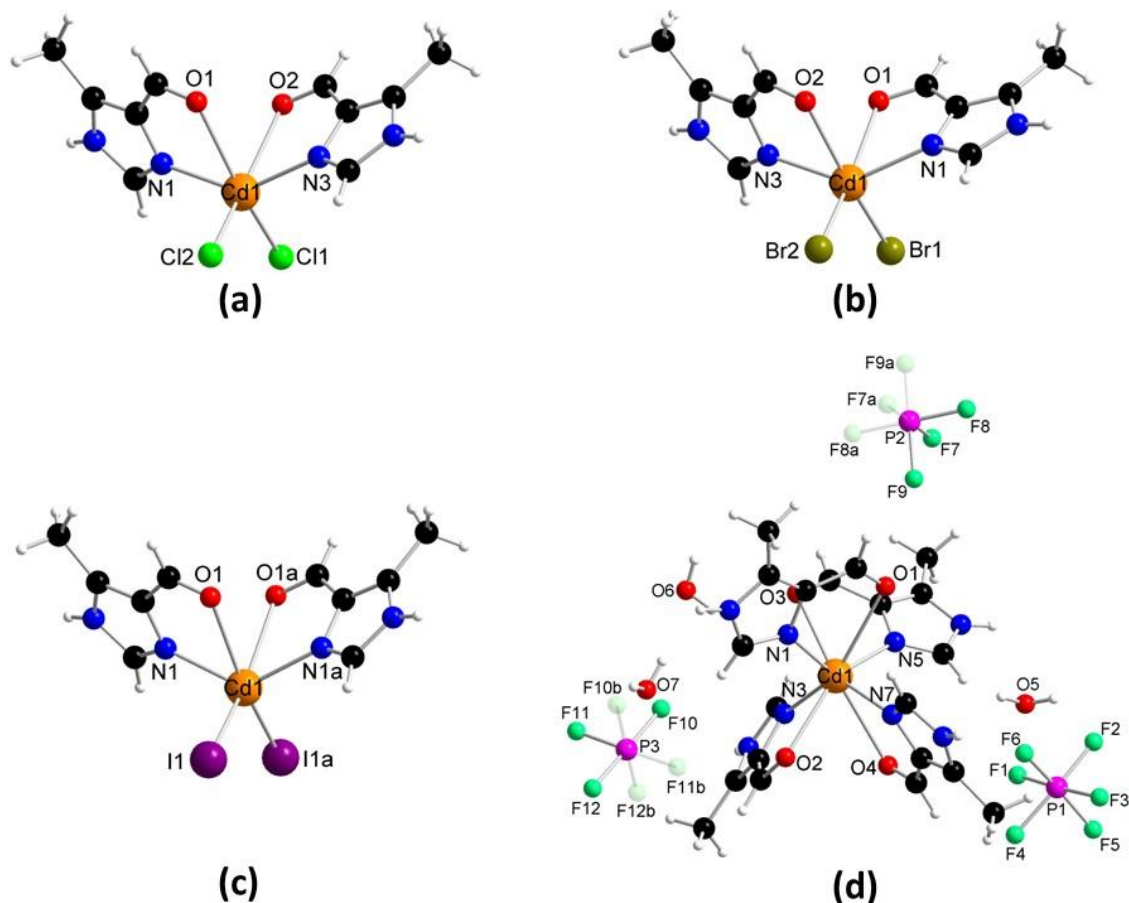


Figure 1. The molecular structures of Cd(II) complexes **1–4** with the atom numbering scheme. [symmetry codes: a = 1-x, y, 0.5-z; b = 1-x, 1.5-y, z].

The crystal packing of complex **1** is provided especially by N–H \cdots Cl and N–H \cdots O hydrogen bonds formed by imidazole N–H groups and chloride ions or carbonyl O-atoms of neighboring molecules (Fig. S5, Table S4). The chains formed in this way are additionally stabilized by $\pi\cdots\pi$ stacking interactions between imidazole rings with inter-centroid distances of 3.441 and 3.504 Å. Interchain interactions are provided by weaker C–H \cdots O or C–H \cdots halogen hydrogen bonds observed also in the crystal structures of **2** and **3**. Similarly, the molecules of complex **2** are arranged in the crystal packing due to the presence of N–H \cdots Br and N–H \cdots O hydrogen bonds (Fig. S6a) supported by $\pi\cdots\pi$ interactions (3.468 Å) (Fig. S6b). In the structure of **3**, there are observed only N–H \cdots O hydrogen bonds between imidazole N–H-donors and aldehyde O-acceptors as well as $\pi\cdots\pi$ stacking interactions at distance 3.735 Å (Fig. S7). The rich H-bonds net in the crystal structure of **4** is formed especially by the presence of PF₆[−] anions and water molecules. There are also observed mentioned above N–H(imidazole) \cdots O(aldehyde) hydrogen bonds (Fig. S8a). The water molecules provided O–H-donors and O-acceptors, while PF₆[−] anions provided F-acceptors for H-bonds (Fig. S8b).

FT-IR analysis

The results of FT-IR comparative analysis for 4-methyl-5-imidazolecarboxaldehyde (**L**) and Cd(II) complexes **1–4** are summarized in Table S5. In the spectrum of the ligand (Figure 2), there is a strong absorption band at 1664 cm^{-1} , which can be attributed to the $\nu(\text{C}=\text{O})$ vibrations in the aldehyde group. This band in the spectra of the complexes is shifted to the lower wavenumbers (in the range $1616\text{--}1623\text{ cm}^{-1}$ for **1–4**, respectively). Calculated spectroscopic $\Delta\nu$ values ($\Delta\nu = \nu_{\text{complex}} - \nu_{\text{ligand}}$) indicates the involvement of O-carbonyl atoms in the coordination to the Cd(II) ion. At the same time, it has been observed some correlation between the $\nu(\text{C}=\text{O})$ band shift and the M–O bond length. Considering the bond lengths (Table S2), this relationship is correctly illustrated by the series: **4** > **3** > **1** > **2** (the larger the metal-oxygen distance, the lower the $\Delta\nu$ value [55, 56], see Table S5). The absorption bands at 1512 and 1439 cm^{-1} in the spectrum of ligand are attributed to the stretching vibrations of the C=C and C=N bonds of the imidazole ring. Analogous bands occur in the spectra of complexes at a slightly higher wavenumbers and $\Delta\nu_{\text{C}=\text{N}}$ in the range $3\text{--}12\text{ cm}^{-1}$ (**1–4**, respectively) confirm the involvement of the imidazole nitrogen atom in the coordination to the Cd(II) ion. Such results correlates with the data obtained by the X-ray method on single crystals (Table S2). Additionally, the band at 3653 cm^{-1} observed in the spectrum of complex **4** indicates the presence of water molecules in the structure. In turn, the presence of PF_6^- anions in the structure of **4** is reflected as a strong vibration band with a maximum of 830 cm^{-1} .

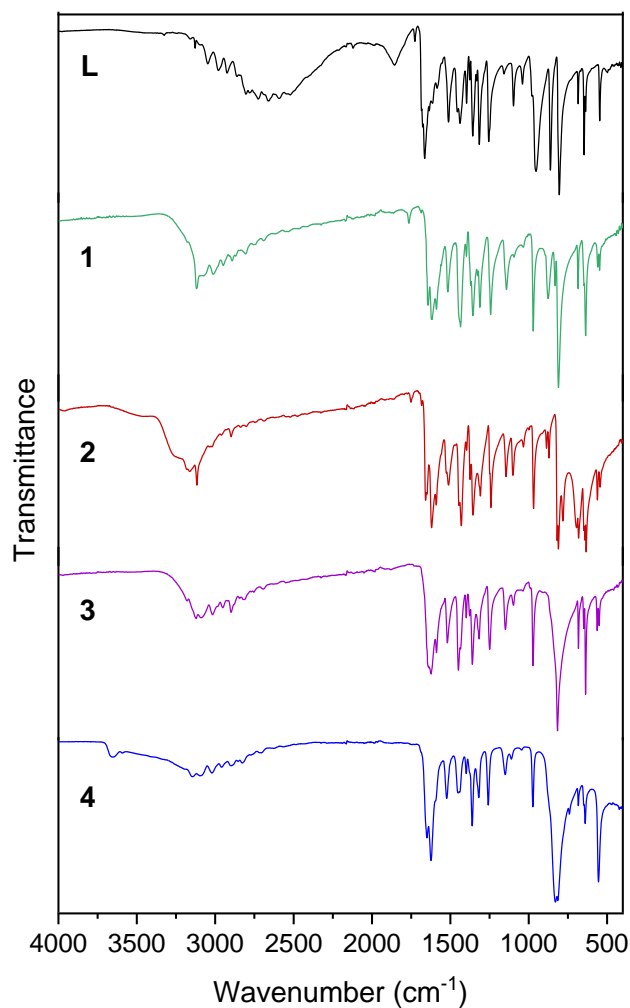


Figure 2. Experimental FT-IR spectra of ligand (**L**) and complexes **1–4**.

UV-Vis stability study

The stability studies were performed for ligand (**L**) and complexes **1–4** dissolved in TE40 buffer ($[L] = 1 \cdot 10^{-4}$ M, $[1-4] = 1 \cdot 10^{-5}$ M) used further in switchSense technique for the determination of interactions with DNA. Figure S9 shows that complexes **1**, **2**, **4** and the free ligand exhibit a single absorption band centred at about 267 nm. For this intense band a weak red shift about 1–2 nm can be observed for the complexes compared to the free ligand and can be attributed to the intraligand $\pi \rightarrow \pi^*/n \rightarrow \pi^*$ transition for the aromatic ring. Moreover, the electronic spectrum of complex **3** show another one band at 225 nm related to the presence of iodine [57] and LLCT transitions [58] arise from iodine ($5p^6$) nonbonding orbitals to the imidazole ring. In the visible region of the spectrum, no band related to d-d transitions is observed that is in accordance with the d^{10} configuration of the Cd(II) ion. In addition, as shown in Figure S9, no changes in band intensities or shifts in band maxima were observed for all tested compounds. This provides a

reliable basis for predicting the stability of the analyzed complexes after dissolution in TE40 buffer.

Computational analysis

The values of dipole moments calculated for studied systems with the use of generalized MP2 densities show that compounds **1–3** are highly polar, and as such are expected to interact with biomolecular receptors to a significant degree. The dipole moment of **4** is not reported here, as for charged species it becomes an origin-dependent quantity. As can be seen in Figure S10 on the example of gas-phase optimized **1–3**, the negative end of the dipole moment vector is always located between two halogen atoms. It can be seen from Table 2 that the calculated dipole moments exceed 12 D in every example. The values of dipole moments calculated for gas-phase relaxed geometries are somewhat smaller than those calculated for crystal structures. This phenomenon is purely related to the changes occurring during the computational optimization of crystal structures. An exemplary angle formed by halogen-cadmium-halogen atoms is a great indicator of geometrical changes, and thus charge distribution variations taking place during relaxation. Namely, optimization leads to a 21.0, 23.5, and 23.3 degrees decrease in said angle for **1**, **2**, and **3**, respectively. Altogether this makes crystal structures more longitudinal or pointy as compared to the gas-phase optimized arrangement. Interestingly, gas-phase optimized structures display trends observed for far lighter analogs of HCl, HBr, and HI, for which dipole moment decreases with the increase of the halogen's atomic number [59]. On the other hand, the exact opposite trend is observed for the dipole moments of **1–3** compounds calculated based on crystal structures.

Table 2.

Dipole moments of **1–3** systems calculated using MP2/aug-cc-pVDZ (Cd and I)/aug-cc-pVDZ (remaining atoms) densities for the geometries obtained using X-ray and optimized computationally.

System	Dipole moment [D]	
	Crystal structure	Gas-phase optimized structure
1	15.758	13.389
2	16.656	13.331
3	17.752	12.884

The molecular electrostatic potential maps provide easy-to-interpret insights into the spatial arrangement of charge densities within a molecule [60]. The maps corresponding to the gas-phase structures of **1–3** are depicted in Figure 3. Due to the charged character of **4**, we have

decided not to show its MEP map, as it is incomparable with the ones corresponding to the remaining compounds. It is clear from the analysis of Figure 3 that three parts of every system stand out in terms of electrostatic potential, and thus are expected to be the main sources of interaction with the surroundings. Namely, the mentioned parts are dative bonded halogen atoms, 1*H*-imidazole hydrogen atom, and oxygen atoms of formyl substituents. As expected, the electrostatic potential on halogen substituents decreases with increasing atomic number, as the corresponding values shrink by $0.015 \text{ e}\cdot\text{\AA}^{-1}$ while going from Cl to I atom. This is related to both decreasing electron affinity as well as the overall electronegativity of parent atoms. On the other side of the electrostatic potential spectrum are the 1*H*-imidazole hydrogen atoms, which due to high values of said potential, namely 0.234, 0.235, and 0.237 $\text{e}\cdot\text{\AA}^{-1}$ for **1**, **2**, and **3** respectively are expected to be the most important deprotonation sites of studied compounds. Close values calculated for discussed H atoms of three discussed compounds indicate that the overall Brønsted acidity of studied systems is independent of halogen substituent. As mentioned earlier, the last part of the studied systems that is noticeable in terms of MEP is the oxygen atoms of imidazole's formyl substituent. The electrostatic potential corresponding to said atoms decreases from -0.077 via -0.078 to $-0.083 \text{ e}\cdot\text{\AA}^{-1}$ while going from **1** to **3**. As such, these are expected to take part in the interactions with the environment as nucleophiles, just as the halogen atoms bonded to the Cd center.

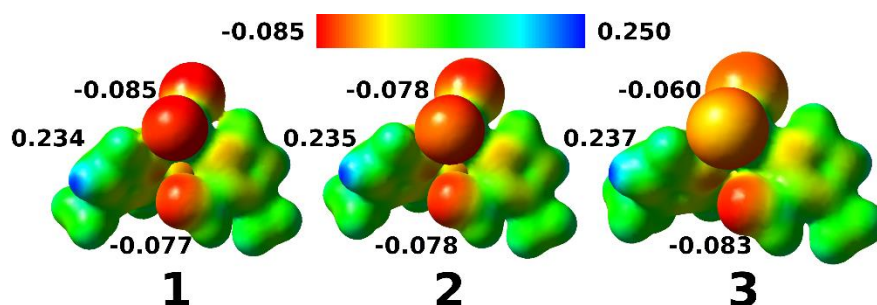


Figure 3. Molecular electrostatic potential maps of gas-phase optimized **1–3** compounds. The calculated electrostatic potential was mapped on an electron density contour with $0.01 \text{ e}\cdot\text{\AA}^{-1}$ isovalue. The values of electrostatic potential are given in $\text{e}\cdot\text{\AA}^{-1}$.

The Gibbs free energies of complex formation are listed in Table 3. As is evident from the results presented in said table, the formation of studied compounds is a highly spontaneous process. As far as the formation of compounds **1–3** was expected to be highly favorable, as it leads to the neutralization of otherwise unstable in gas-phase divalent Cd(II), the significantly negative ΔG_{stb} calculated for divalent cation of **4** is somewhat surprising. What's even more unanticipated is that **4**'s thermodynamic stability is higher than that of **2** and **3**. While ΔG_{stb} of

1, **2**, and **4** are somewhat close to $-570 \text{ kcal}\cdot\text{mol}^{-1}$, that of **3** is slightly smaller and equal to $-560 \text{ kcal}\cdot\text{mol}^{-1}$. The stability constants (β) corresponding to studied systems are expected to follow the same trend.

Table 3.

Gas-phase Gibbs free energies of formation (ΔG_{stb}) of studied coordination compound systems calculated at 298.15 K (in $\text{kcal}\cdot\text{mol}^{-1}$) for the reaction presented in eq. 1.

System	ΔG_{stb}
1	-573.0
2	-568.2
3	-557.3
4	-570.6

Another way to assess a coordination compound's stability is to compute the multiplicity of dative bonds formed within the complex. To do that we have decided to conduct FBO analysis. The results of which are collected in Table S6. The FBO analysis reveals a clear pattern when it comes to the number of electron pairs between two bonded atoms. Namely, regardless of the type of structure considered or the compounds the FBO decreases in the following order Cd-halogen > Cd-nitrogen > Cd-oxygen. The values of FBO calculated for Cd-halogen bonds exceed 1.100 in every example and in some examples take as high values as 1.319 and 1.230 for gas-phase and crystal structures, respectively. The values of the FBO index calculated for Cd-N are considerably smaller and fall between 0.692 and 0.833 (gas-phase) and in 0.774–0.851 intervals (crystal). The Cd-O type bonds are the weakest among all of the types discussed here. The corresponding FBOs do not exceed 0.372 and 0.543 for the two considered phases. As such they should rather be considered as van der Waals interactions than coordinate bonds.

The eigenvalues of frontier orbitals corresponding to studied systems are presented in Figure S11. The significant values of HOMO–LUMO gaps (none is smaller than 7.500 eV) indicate the high electronic stability of studied coordination compounds. The discussed gaps calculated for gas-phase structure are 0.722, 1.065, and 0.890 eV higher than those determined for crystal structures of **1**, **2**, and **3** respectively. The highly negative eigenvalues of HOMO orbitals indicate a high resistance of studied systems towards oxidation processes. The eigenvalues of LUMO orbitals calculated for all systems but **1** in the crystal structure are all close to zero indicating significant reactivity of studied compounds towards both reduction and general reactions where those compounds act as electron density acceptors - nucleophiles.



The molecular volume of a potential drug is among the important traits when it comes to pharmaceutical activity. It affects the drug's delivery to the system, pharmacokinetics, and interaction with biological targets and can affect e.g. blood-brain barrier penetration. The calculated volumes of all systems studied in this paper are listed in Table S7. Compounds **1–3** are characterized by volumes in the 349–405 Å³ range, with volume increasing along with the atomic number of halogen substituents. As such, they have volume similar to popular drugs such as fluoxetine or morphine [60]. It can be seen from said table that the differences in molecular volumes between crystal and gas-phase structures are negligible for compounds **1–3**, and are equal to circa 12 Å³. The molecular volume of **4** is significantly larger, as it was calculated to be 537.67 and 849.80 Å³ for gas-phase and crystal structure, respectively. With its volume equal to 537.67 Å³ **4** has a volume comparable to that of tetracycline or nifedipine [61].

Another factor that affects the pharmaceutical's fate within a human body is its polarity. One way to assess that is to determine the partition coefficient. This is a hard computational task as it requires a correct assessment of the Gibbs free energies of solvation. Another, rather novel method employed to assess the polarity of a given compound is to calculate the so-called Molecular Polarity Index, which is getting more and more attention nowadays [62–64]. The values of MPI calculated for systems studied here are collected in Table S8. The values of MPI calculated for gas-phase structures of **1** and **2** are close to 28 kcal·mol⁻¹, whereas that of **3** is smaller by circa 1 kcal·mol⁻¹. As expected, the corresponding values calculated for crystal structures are slightly higher and in 33–35 kcal·mol⁻¹ range. The values of MPI for charged system **4** although not listed in the table since their non-zero net charge make them incomparable with the remaining compounds. To get an idea of the polarity of the studied system, the values of MPI calculated for water, ethanol, and hexane at B3LYP-D3/Def2-QZVP level of theory by Ye et al., were found to be equal to 21.24, 11.17 and 2.84 kcal·mol⁻¹ respectively [63]. Whereas that of the MPI of tinidazole, an antibacterial and antiprotozoal pharmaceutical calculated at B3LYP/6-311G+(d,p) was calculated to 20.20 kcal·mol⁻¹ [65]. With all of that in mind, it seems that the compounds studied in this work are highly polar, regardless of the origin of the structure considered. This concurs well with the high values of dipole moments discussed in previous parts of the manuscript.



Affinity to DNA (switchSense technique)

Kinetic analysis using the switchSense technique began with examining the ligand (5-methyl-4-imidazolecarboxaldehyde) molecule at 25 °C. The resulting graph (Fig. S12) shows slight changes in fluorescence intensity throughout the measurement. No significant changes are observed after initiation of either the association or dissociation process. Too small changes made it impossible to determine any kinetic parameters (k_a , k_d , K_A , or K_D). Based on the information obtained, it can be assumed that the formation of a ligand–DNA adduct does not occur or that the technique discussed is not an appropriate method to study such an interaction. We intend to test this hypothesis using other techniques in the future. Therefore, further detailed measurements of the ligand molecule at other temperatures using the switchSense method were discontinued.

A completely different situation occurs when examining the interactions of Cd(II) complexes with the mentioned ligand. The curves illustrating the process of association and dissociation of complex **1** containing chloride ligands to a double-stranded DNA fragment are shown in Figure 4. Negative values of the fluorescence change mean a decrease in the fluorescence intensity of the signaling unit during the measurements. After the buffer flow time has elapsed (about 20 s), there is a sharp decline in the curve related to the process of association with the DNA molecule and its subsequent dissociation (about 180 s). This proves that both the formation of the **1**–DNA adduct and its subsequent dissociation occur very quickly. At all analyzed temperatures, the shape of the curve is very similar. However, as the temperature increases, the intensity of the fluorophore signal decreases even more. It is proportionally more intense, the higher the concentration of the analyte being tested. At a temperature of 37 °C for a concentration of $1.6 \cdot 10^{-3}$ M fluorescence intensity drops to about –60%. A flat section between approximately 20 and 180 s of measurement indicates that no further analyte molecules are attached and therefore the association process is considered exhausted and completed. In all analyzed temperatures, the change in fluorescence intensity increases again to approximately 0%, as a result of the dissociation process, which proves the complete dissociation of complex molecules from the DNA helix as a result of washing with buffer.

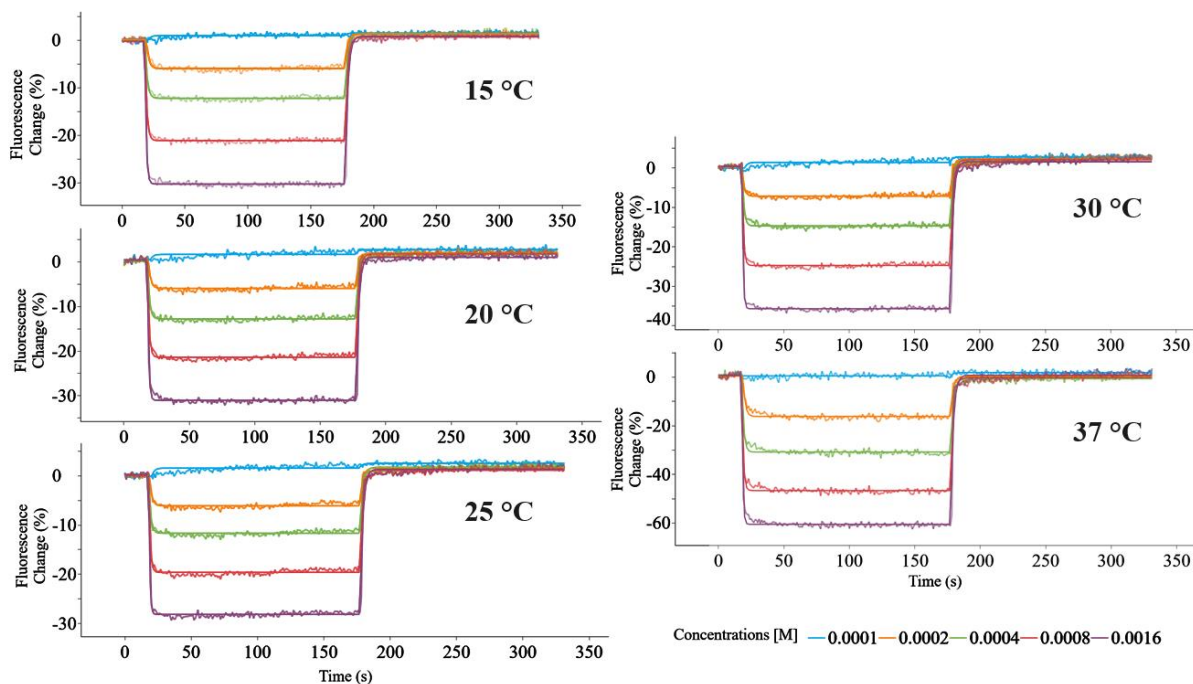


Figure 4. Representative results showing changes in fluorescence over time occurring during the analysis of the interactions of the complex **1** with the DNA helix performed in the static mode (weak binders) at temperatures: 15, 20, 25, 30, and 37 °C. The thinner lines in each color represent the measurement points and the bold line represents the fitted data from which the kinetic parameters are calculated.

For the remaining three tested compounds **2–4** (please see Figures S13–S15, respectively), the resulting curve data depicting the ongoing interaction processes exhibit identical trends to those observed with the complex **1**. The only differences are noticed in the decrease in fluorescence intensity. The maximum negative values are slightly lower than in the case of the first complex, while the shape of the curve of association and dissociation processes is maintained. These graphs illustrate a very similar nature of the interaction of all complexes with DNA, regardless of the type of anion present in the coordination sphere (Cl^- , Br^- , I^-) or outside of it (PF_6^-).

The data obtained from three independent replicate experiments for all analytes were repeatable. All determined values of kinetic parameters are presented in Table 4. It can be noticed that the increase in temperature has a small impact on the rate of association processes (increase in k_a value). The values indicate a slower binding of these compounds to DNA than in the case of the intercalator well-known in the literature ethidium bromide ($k_a = 1.03 \pm 0.19 \cdot 10^6 \text{ M}^{-1} \cdot \text{s}^{-1}$ at 37 °C) [36]. There are no significant differences in the dissociation rate of the formed adduct due to temperature changes (k_d value). Similar rate values are mainly determined by the buffer flow. The determined values of binding constants (K_A) increase with increasing temperature. The highest value obtained for compound **1** is over $1 \cdot 10^3 \text{ M}^{-1}$, which might

indicate interaction in the small groove of DNA. This assumption can be made based on the study conducted previously in our group [36] in which low-molecular-weight compounds with DNA using both the switchSense and docking techniques showed that the association constant K_A was of the order of $1 \cdot 10^3$ M. The conclusions resulting from the docking suggested the interaction of the tested compounds in the minor groove of DNA.

Table 4.

Values (along with their standard deviations in the parentheses) of determined association rates k_a (in $[M^{-1} \cdot s^{-1}]$), dissociation rates k_d (in $[s^{-1}]$), associations constants K_A (in $[M^{-1}]$), and dissociation constants K_D (in $[M]$) for complexes **1–4** interactions with DNA measured by switchSense technique at five different temperatures 15, 20, 25, 30, and 37 °C, respectively.

Compound	Temp. [°C]	k_a [$M^{-1} \cdot s^{-1}$]	k_d [s^{-1}]	K_A [M^{-1}]	K_D [M]
1	15	275 ± 24	$(5.04 \pm 0.11) \cdot 10^{-1}$	546 ± 49	$(1.83 \pm 0.17) \cdot 10^{-3}$
	20	394 ± 33	$(5.34 \pm 0.12) \cdot 10^{-1}$	737 ± 65	$(1.36 \pm 0.12) \cdot 10^{-3}$
	25	557 ± 46	$(5.17 \pm 0.12) \cdot 10^{-1}$	$(1.08 \pm 0.09) \cdot 10^3$	$(9.28 \pm 0.80) \cdot 10^{-3}$
	30	534 ± 67	$(5.29 \pm 0.12) \cdot 10^{-1}$	$(1.01 \pm 0.13) \cdot 10^3$	$(9.91 \pm 1.27) \cdot 10^{-4}$
	37	589 ± 48	$(5.18 \pm 0.12) \cdot 10^{-1}$	$(1.14 \pm 0.10) \cdot 10^3$	$(8.80 \pm 0.74) \cdot 10^{-4}$
2	15	315 ± 32	$(6.24 \pm 0.16) \cdot 10^{-1}$	505 ± 52	$(1.98 \pm 0.21) \cdot 10^{-3}$
	20	520 ± 88	$(5.77 \pm 0.17) \cdot 10^{-1}$	901 ± 155	$(1.11 \pm 0.19) \cdot 10^{-3}$
	25	361 ± 29	$(4.94 \pm 0.11) \cdot 10^{-1}$	731 ± 61	$(1.37 \pm 0.11) \cdot 10^{-3}$
	30	582 ± 36	$(5.05 \pm 0.10) \cdot 10^{-1}$	$(1.15 \pm 0.07) \cdot 10^3$	$(8.68 \pm 0.56) \cdot 10^{-4}$
	37	658 ± 47	$(4.95 \pm 0.11) \cdot 10^{-1}$	$(1.33 \pm 0.10) \cdot 10^3$	$(7.53 \pm 0.56) \cdot 10^{-4}$
3	15	179 ± 37	$(6.74 \pm 0.26) \cdot 10^{-1}$	265 ± 56	$(3.78 \pm 0.80) \cdot 10^{-3}$
	20	246 ± 74	$(6.25 \pm 0.17) \cdot 10^{-1}$	394 ± 119	$(2.54 \pm 0.77) \cdot 10^{-3}$
	25	282 ± 82	$(6.42 \pm 0.22) \cdot 10^{-1}$	439 ± 128	$(2.28 \pm 0.66) \cdot 10^{-3}$
	30	445 ± 80	$(6.50 \pm 0.21) \cdot 10^{-1}$	685 ± 125	$(1.46 \pm 0.27) \cdot 10^{-3}$
	37	479 ± 40	$(5.34 \pm 0.13) \cdot 10^{-1}$	898 ± 77	$(1.11 \pm 0.10) \cdot 10^{-3}$
4	15	266 ± 19	$(4.47 \pm 0.09) \cdot 10^{-1}$	594 ± 44	$(1.68 \pm 0.12) \cdot 10^{-3}$
	20	323 ± 23	$(3.97 \pm 0.08) \cdot 10^{-1}$	814 ± 59	$(1.23 \pm 0.09) \cdot 10^{-3}$
	25	371 ± 36	$(4.28 \pm 0.09) \cdot 10^{-1}$	865 ± 86	$(1.16 \pm 0.11) \cdot 10^{-3}$
	30	713 ± 45	$(3.94 \pm 0.09) \cdot 10^{-1}$	$(1.81 \pm 0.12) \cdot 10^3$	$(5.52 \pm 0.37) \cdot 10^{-4}$
	37	742 ± 60	$(4.07 \pm 0.10) \cdot 10^{-1}$	$(1.82 \pm 0.15) \cdot 10^3$	$(5.49 \pm 0.47) \cdot 10^{-4}$

To sum up, the determined kinetic parameters for all the studied complexes have the same order of magnitude. In all cases association process dominates over dissociation. There are no significant differences in the rate of association processes or binding constant that could result from the addition of another anion to the ligand. Unlike the ligand molecule itself, all its coordination connections with Cd(II) interact with the DNA molecule. The analysis shows that combinations of metals (in our case Cd(II)) with an appropriate ligand, can increase the biological activity of such a molecule [24, 25].

A kinetic analysis at 25 °C was also performed for the CdCl₂ salt itself, which was the source of Cd²⁺ ions in complex **1**. The obtained curve has a very similar shape to that for complex **1** under the same measurement conditions (Figure S16). The difference only occurs in the fluorescence intensity of the signaling unit. For the highest concentration of complex **1** (1.6·10⁻³ M) the fluorescence intensity drops to about -30%, while for the salt it is about -22%. Obtained, among others: the values of the association rate (k_a) and the association constant (K_A) are lower for the salt (Table S10) than for complex **1**, while none of the parameters was determined for the ligand itself. This is another proof that the complexation of metal ions (in this case Cd²⁺) increases the biological activity of the newly obtained compounds. This is also observed by an increase in association constants by about 50% [13].

All values of the determined thermodynamic parameters for the studied complexes are listed in Table S9 and were computed as given in eqs. 4–6, respectively. The obtained ΔG values for all compounds are negative, and they further decrease with increasing temperature (Figures S17a, S18a, S19a, and S20a), which suggests the spontaneous nature of the formed systems. The entropy change ΔS for all tested systems is positive (Figures S17b, S18b, S19b, and S20b), which would indicate that the initial state is more ordered than the final state. The exception is the ΔS value for **2** at 25 °C (Figure S18b), where the value is -0.05 kJ·mol⁻¹. This may suggest an increase in the order of the adduct being formed at a given temperature. For the tested compounds, the ΔH value is positive at most temperatures, which suggests an endothermic process. However, for **1** at 30 °C it reaches a minimum value (-10.06 kJ·mol⁻¹), and for **2** at 25 °C (-30.34 kJ·mol⁻¹) (Figures S17c and S18c). For complex **3**, the minimum ΔH value occurs at 25 °C and for **4** at 37 °C, and for neither of them, it reaches a negative value (Figures S19c and S20c).

A relationship between both experimentally obtained and calculated Gibbs free energy changes of complex formation process at 298 K has been shown in Figure 5. There is a very good agreement observed with a quite high value of $R^2 = 0.9783$. This suggests also that the theoretical model reproduces experimental results qualitatively well.

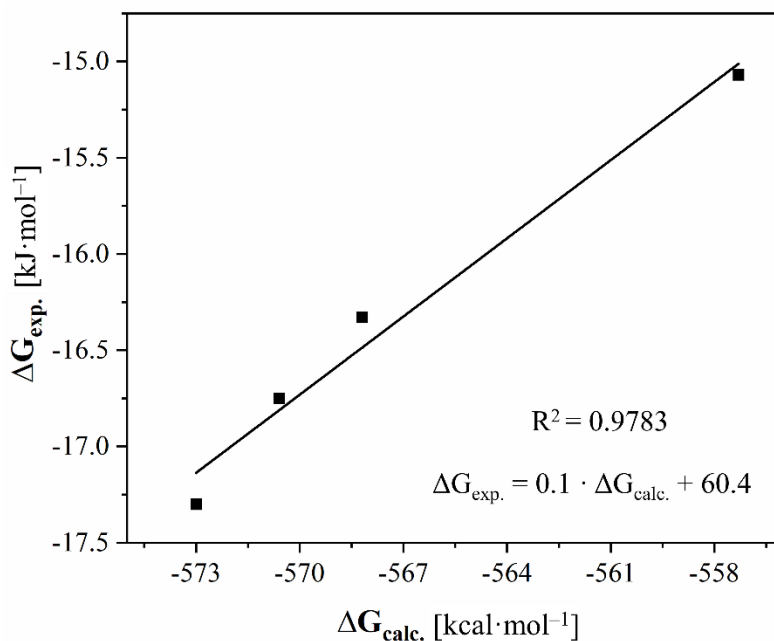


Figure 5. Correlation plot between $\Delta G_{\text{calc.}}$ and $\Delta G_{\text{exp.}}$. Black squares refer to data, and a solid line is a linear regression.

Conclusions

In summary, the synthesis and characterization of a series of Cd(II) complexes (**1–4**) have been successfully achieved through one-step and two-step reactions using Cd(II) chloride and Cd(II) acetate, respectively, along with 5-methyl-4-imidazolecarboxaldehyde (**L**) as a ligand. The obtained complexes were isolated as stable colorless crystals. Their structural analysis revealed distinct coordination environments for each complex, with variations in bond lengths and angles. Notably, complexes **1–3** featured octahedral CdX_2L_2 units (where $\text{X} = \text{Cl}^-$, Br^- , or I^-), while complex **4** exhibited a cationic $[\text{CdL}_4]^{2+}$ dodecahedral structure. The crystal packing of the complexes was stabilized by hydrogen bonding and π - π stacking interactions, contributing to their structural stability. FT-IR analysis confirmed the coordination of the ligand to the metal ion in the complexes, while the UV-Vis study demonstrated their stability in solution. Computational analysis revealed the polar nature of the complexes with dipole moments ca. 15–17 D for **1–3**, along with favorable stability constants. Affinity studies with DNA using the switchSense technique indicated rapid association and dissociation processes for all complexes, with temperature-dependent binding constants. The highest binding constants observed for all Cd(II) coordination connections, except complex **3**, are approximately within the same order of magnitude (10^3 M^{-1}), suggesting a potential similarity in their interactions with DNA. This concurs with the results obtained via computational approach, as **3** complex was characterized

by the lowest values of dipole moment and as such was expected to interact with DNA to a lesser extent than remaining systems. The relatively low values of electrostatic potential corresponding to the halide atoms of **3** located on the negative end of dipole moment vector further prove described expectations. Among the complexes with varying anions in their coordination sphere (**1–3**), slight discrepancies in K_A values were noted. Notably, complex **3**, incorporating the I^- anion, exhibits slightly diminished kinetic parameter values compared to those with Cl^- and Br^- anions. Correlation of bond lengths and valence angles in complexes **1–3** shows that the length of Cd–halogen bonds increases with the increase in the atomic radius of a given halogen. A comparative analysis of the Cd–O and Cd–N bond lengths in the studied complexes shows that the longest bond with the oxygen atom (2.71 Å) occurs in complex **3**. In contrast, the Cd–N bond length (2.27 Å) is shorter than the Cd–O bond. This may result from the coordination preference of the soft Cd(II) ion towards the softer N-donor atom according to HSAB theory. This difference in bond lengths is responsible for the significant variation in valence angles and distortion of the coordination polyhedron compared to the other compounds. However, this does not differentiate the activity of the compounds. It can be also noted that the molecule of complex **3** does not form as many hydrogen bonds or non-covalent interactions as complexes **1** and **2** due to the reduced electronegativity and large van der Waals radius of the iodide ligands. This may therefore suggest a less effective binding or interaction of complex **3** with DNA in the proposed model of non-covalent groove interactions under the conditions of the experiment conducted. However, a more detailed elucidation of the mode of action of the Cd(II) complexes obtained and the reasons for the differential biological activity of complexes **1–3** will require further follow-up studies. The highest binding constant across all complexes was determined for compound **4**, which features the PF_6^- anion located outside the coordination sphere. This implies that the increase in the electronegativity of halogen elements could affect their ability to bind biomolecules. Additionally, compound **4**, being a cationic complex, could potentially enhance the binding constant with DNA by interacting with negatively charged phosphate groups. Nevertheless, further investigation is essential to substantiate these conjectures. The thermodynamic analysis additionally confirmed the spontaneous and endothermic nature of complex formation processes with a positive entropy change. Overall, it can be concluded that the synthesized Cd(II) complexes exhibit promising characteristics for potential applications in medicinal chemistry.

Understanding the interaction between chemical compounds, especially metal complexes, and DNA is crucial in medicinal chemistry, enabling diverse applications such as anticancer



therapy, gene regulation, and antimicrobial activity. Metal complexes with high DNA-binding affinity can be customized to enhance efficacy and selectivity in designing DNA-targeted therapeutics, offering promise for targeted gene therapy and as candidates for new antibiotics. Moreover, compounds with strong DNA-binding affinity can aid in diagnostic techniques by facilitating the visualization and detection of specific DNA sequences. The observed kinetic parameters and binding constants of the synthesized Cd(II) complexes offer valuable insights into their biological activity and therapeutic potential. Their rapid association and dissociation kinetics with DNA suggest dynamic interactions, particularly beneficial in anticancer therapy, capable of disrupting cellular processes and inhibiting tumor growth. High binding constants indicate strong affinity between the complexes and DNA, crucial for their effectiveness in inhibiting DNA replication or transcription in cancer cells, while also suggesting potential antimicrobial activity against drug-resistant bacteria. The increase in binding constants with temperature suggests enhanced interaction at higher temperatures, indicative of thermodynamic stability. Comparison with reference compounds confirms their potential as therapeutic agents, while consistency across complexes underscores their robust DNA-binding properties, facilitating predictable pharmaceutical development.



ACKNOWLEDGMENTS

This work was supported by the Polish National Science Centre (NCN) under a grant UMO-2019/33/B/ST4/00031. The financial support for maintenance of research facilities used in these studies from Gdańsk University of Technology by the DEC-2/2021/IDUB/V.6/Si grant under the SILICIUM SUPPORTING CORE R&D FACILITIES – “Excellence Initiative - Research University” program is gratefully acknowledged.

SUPPLEMENTARY INFORMATION

Supplementary Information file contains **Table S1**: Cartesian coordinates of the gas-phase optimized structures of compounds **1–4**; **Table S2**: Bond lengths for complexes **1–4** obtained from X-ray analysis; **Table S3**: Valence angles for complexes **1–4** obtained from X-ray analysis; **Table S4**: The geometry of the most important hydrogen bonds in the crystal structures of complexes **1–4**; **Table S5**: Selected FT-IR spectroscopic data for ligand and complexes **1–4**; **Table S6**: Results of the FBO analysis of the bonds formed by Cd(II) ion within the studied coordination compounds; **Table S7**: The molecular volumes of **1–4** systems calculated numerically with the use of marching tetrahedra method; **Table S8**: The values of Molecular Polarity Index of **1–4** systems; **Table S9**: The determined values of thermodynamic parameters ΔG , ΔH , and ΔS for **1–4** are based on their association constant K_A ; **Table S10**: Values of determined association rates k_a , dissociation rates k_d , associations constants K_A , and dissociation constants K_D for salt CdCl_2 interactions with DNA measured by switchSense technique at temperature 25 °C. **Figs. S1–S4**: The ESI-MS spectrograms of complexes **1–4**; **Figs. S5–S8**: The geometry of non-covalent interactions in the crystal structures of complexes **1–4**; **Fig. S9**: The stability studies of ligand and complexes **1–4** in TE40 buffer monitored by UV-Vis; **Fig. S10**: The equilibrium geometries of gas-phase optimized **1–3** compounds with corresponding dipole moment vectors; **Fig. S11**: The eigenvalues of **1–3** compounds' frontier orbitals; **Fig. S12**: Result showing changes in fluorescence over time occurring during the analysis of the interactions of the ligand with the DNA helix performed in the static mode (weak binders) at temperature 25 °C; **Figs. S13–S15**: Representative results showing changes in fluorescence over time occurring during the analysis of the interactions of the complexes **2–4** with the DNA helix performed in the static mode (weak binders) at temperatures: 15, 20, 25, 30, and 37 °C; **Fig. S16**: Result showing changes in fluorescence over time occurring during the analysis of the interactions of CdCl_2 with the DNA helix performed in the static mode (weak binders) at temperature 25 °C; **Figs. S17–S20**: Dependence of the change of a) Gibbs free energy (ΔG), b) enthalpy (ΔH), and c) entropy (ΔS) as a function of temperature for the complexes **1–4**.

AUTHORS' CONTRIBUTION STATEMENT

M. Kowalik: conceptualization of a whole work, discussion of the results, writing a significant part of the original draft, correction of the original draft, synthesis, physicochemical and structural characterization of compounds; **P. Nowicka**: conceptualization in part, writing the original draft in part, studies of interactions with DNA (switchSense technique); **J. Brzeski**: conceptualization in part, writing the original draft in part, computational analysis; **N. Żukowska**: synthesis, FT-IR analysis; **J. Masternak**: solution stability studies, correction of



the original draft; **K. Kazimierzuk**: X-ray diffraction measurements; **M. Makowski**: conceptualization in part, supervision, funds acquisition, writing the original draft in part, correction of the original draft.

All authors have edited, reviewed, corrected, and accepted the final version of the article.

DECLARATION OF COMPETING INTERESTS

The authors declare that they have no known competing financial interests or personal relationships that could have appeared to influence the work reported in this paper.

REFERENCES

- [1] G. Genchi, M. S. Sinicropi, G. Lauria, A. Carocci, A. Catalano, *Int. J. Environ. Res. Public Health*, 2020, **17**, 3782.
- [2] B. A. O. Al-Ameen, A. R. Khalid, A. J. M. Al-Karawi, S. Marah, S. Kansız, Y. Sert, M. I. Jaafar, N. Dege, E. B. Poyraz, A. M.A. Ahmed, T. Ozen, M. Loukil, R. S. Jwad, *J. Mol. Struct.*, 2023, **1290**, 135974.
- [3] D. N. Hume, D. D. DeFord, G. C. B. Cave, *J. Am. Chem. Soc.*, 1951, **73**, 5323–5325.
- [4] F. Jalilehvand, B. O. Leung, V. Mah, *Inorg Chem.*, 2009, **48**, 5758–5771.
- [5] I. Warad, M. Azam, S. I. Al-Resayes, M. S. Khan, P. Ahmad, M. Al-Nuri, S. Jodeh, A. Husein, S. F. Haddad, B. Hammouti, M. Al-Noaimi, *Inorg. Chem. Comm.*, 2014, **43**, 155–161.
- [6] K.K. Sarker, D. Sardar, K. Suwa, J. Otsuki, C. Sinha, *Inorg. Chem.* 2007, **46**, 8291–8301.
- [7] C.-X. Xu, J.-G. Z., X. Yin, X. Jin, T. Li, T.-L. Zhang, Z.-N. Zhou, *J. Sol. State Chem.*, 2015, **226**, 59–65.
- [8] C. Hopa, H. Yildirim, H. Kara, R. Kurtaran, M. Alkan, *Spectrochim. Acta A: Mol. Biomol. Spectrosc.*, 2014, **121**, 282–287.
- [9] B. Barszcz, J. Masternak, M. Hodorowicz, E. Matczak-Jon, A. Jabłonska-Wawrzycka, K. Stadnicka, K. Królewska, J. Kaźmierczak-Barańska, *Inorg. Chim. Acta.*, 2013, **399**, 85–94.
- [10] A. Raducka, M. Swiatkowski, I. Korona-Głowniak, B. Kapron, T. Plech, M. Szczesio, K. Gobis, A. Czyłkowska, *Pharmaceutics*, 2022, **14**, 1626.
- [11] M. Peana, A. Pelucelli, C. T. Chasapis, S. P. Perlepes, V. Bekiari, S. Medici, M. A. Zoroddu, *Biomolecules*, 2023, **13**, 36.
- [12] K. S. Egorova, V. P. Ananikov, *Organometallics*, 2017, **36**, 4071–4090.
- [13] P. Spisz, A. Chylewska, A. Królicka, S. Ramotowska, A. Dąbrowska, M. Makowski, *Int. J. Mol. Sci.*, 2021, **22**, 13482.
- [14] S. Bjelogrić, T. R. Todorović, I. Cvijetić, M. V. Rodić, M. Vujčić, S. Marković, J. Araškov, B. Janović, F. Emhemmed, C. D. Muller, N. R. Filipović, *J. Inorg. Biochem.*, 2019, **190**, 45–66.
- [15] R. Manikandan, N. Chitrapriya, Y. J. Jang, P. Viswanathamurthi, *RSC Adv.*, 2013, **3**, 11647–11657.
- [16] M. Ravi, K. P. Chennam, B. Ushaiah, R. K. Eslavath, S. Perugu, R. Ajumeera, Ch. S. Devi, *J. Fluoresc.*, 2015, **25**, 1279–1296.
- [17] H.-Y. Luo, J.-Y. Li, Y. Li, L. Zhang, J.-Y. Li, D.-Z. Jia, G.-C. Xu, *RSC Adv.*, 2016, **6**, 114997–115009.
- [18] L. Tabrizi, R. Golbang, H. Sadeghi, H. Chiniforoshan, P. Mcardle, B. Notash, *J. Coord. Chem.*, 2016, **69**, 3021–3034.
- [19] Y. Yang, C.-G. Li, X.-J. Luo, Z.-H. Luo, R.-J. Liu, Y.-X. Jiang, W.-J. Liang, *Supramolecular Chemistry*, 2015, **27**, 281–286.
- [20] N. Zhang, Y. Fan, G. Huang, D. Buac, C. Bi, Y. Ma, X. Wang, Z. Zhang, X. Zhang, Q. P. Dou, *Inorg. Chim. Acta*, 2017, **466**, 478–485.
- [21] A. Chidambaram, A. Sekar, K. S.H., R. K. Chidambaram, K. Arunachalam, S. G.P., R. Vilwanathan, *Invest. New Drugs*, 2017, **35**, 691–705.
- [22] X. Chen, J. Wu, Q. Yang, X. Zhang, P. Zhang, S. Liao, Z. He, X. Wang, C. Zhao, J. Liu, *Biometals*, 2018, **31**, 29–43.

- [23] D.-D. Yang, Y.-N. Chen, Y.-S. Wu, R. Wang, Z.-J. Chen, J. Qin, S.-S. Qian, H.-L. Zhu, *Bioorg. Med. Chem. Lett.*, 2016, **26**, 3295–3299.
- [24] S. B. Marković, N. Maciejewska, M. Olszewski, A. Višnjevac, A. Puerta, J. M. Padrón, I. Novaković, S. Kojić, H. S. Fernandes, S. F. Sousa, S. Ramotowska, A. Chylewska, M. Makowski, T. R. Todorović, N. R. Filipović, *Eur. J. Med. Chem.*, 2022, **238**, 114449.
- [25] S. B. Kokanov, N. R. Filipović, A. Višnjevac, M. Nikolić, I. Novaković, G. Janjić, B. B. Holló, S. Ramotowska, P. Nowicka, M. Makowski, Ö. Uğuz, A. Koca, T. R. Todorović, *Appl. Organomet. Chem.*, 2023, **37**, e6942.
- [26] S. Nasiri Sovari, F. Zobi, *Chemistry*, 2020, **2**, 418–452.
- [27] E. M. Abdalla, L. H. Abdel Rahman, A. A. Abdelhamid, M. R. Shehata, A. A. Allothman, A. Nafady, *Appl. Organomet. Chem.*, 2020, **34**, e5912.
- [28] D. C. Reis, A. A. R. Despaigne, J. G. Da Silva, N. F. Silva, C. F. Vilela, I. C. Mendes, J. A. Takahashi, H. Beraldo, *Molecules*, 2013, **18**, 12645–12662.
- [29] A. K. Gopalakrishnan, S. A. Angamaly, M. P. Velayudhan, *ChemistrySelect*, 2021, **6**, 10918–10947.
- [30] G. A. Krishna, T.M. Dhanya, A.A. Shanty, K.G. Raghu, P.V. Mohanan, *J. Mol. Struct.*, 2023, **1274**, 134384.
- [31] M. K. Yadav, S. Pokhrel, P. N. Yadav, *J. Macromol. Sci. Part A*, 2020, **57**, 703–710.
- [32] E. Orhan, M. Kose, D. Alkan, L. Öztürk, *JOTCSA*, 2019, **6**, 373–382.
- [33] A. Jabłońska-Wawrzycka, B. Barszcz, M. Zienkiewicz, M., Hodorowicz, J. Jezierska, K. Stadnicka, Ł. Lechowicz, W. Kaca, *Spectrochim. Acta A: Mol. Biomol. Spectrosc.*, 2014, **129**, 632–642.
- [34] M. Kowalik, J. Brzeski, M. Gawrońska, K. Kazimierczuk, M. Makowski, *CrystEngComm*, 2021, **23**, 6137–6162.
- [35] M. Kowalik, J. Masternak, M. Olszewski, N. Maciejewska, K. Kazimierczuk, J. Sitkowski, A. M. Dąbrowska, A. Chylewska, M. Makowski, *Inorg. Chem.*, 2024, **63**, 1296–1316.
- [36] S. Ramotowska, P. Spisz, J. Brzeski, A. Ciesielska, M. Makowski *J. Phys. Chem. B*, 2022, **126**, 7238–7251.
- [37] STOE & Cie GmbH. X-area 1.75, *Software Package for Collecting Single-Crystal Data on STOE Area-Detector Diffractometers, for Image Processing, Scaling Reflection Intensities and for Outlier Rejection*; STOE & Cie GmbH: Darmstadt, Germany, 2015.
- [38] G. M. Sheldrick, *Acta. Crystallogr. A*, 2015, **71**, 3–8.
- [39] O. V. Dolomanov, L. J. Bourhis, R. J. Gildea, J. A. K. Howard, H. Puschmann, *J. Appl. Crystallogr.* **2009**, **42**, 339–341.
- [40] G. M. Sheldrick, *Acta. Crystallogr. C*, 2015, **71**, 3–8.
- [41] K. Brandenburg, K. Putz, *Diamond-Crystal and Molecular Structure Visualisation; Crystal Impact; 3.1 G*: Rathausgasse 30, GbR, Bonn, Germany, 1997.
- [42] T. H. Dunning, *J. Chem. Phys.*, 1989, **90**, 1007–1023.
- [43] D. E. Woon, T. H. Dunning, *J. Chem. Phys.*, 1993, **98**, 1358–1371.
- [44] D. Figgen, G. Rauhut, M. Dolg, H. Stoll, *Chem. Phys.*, 2005, **311**, 227–244.
- [45] K. A. Peterson and C. Puzzarini, *Theor. Chem. Acc.*, 2005, **114**, 283–296.



- [46] M. J. Frisch, G. W. Trucks, H. B. Schlegel, G. E. Scuseria, M. A. Robb, J. R. Cheeseman, G. Scalmani, V. Barone, B. Mennucci, G. A. Petersson, H. Nakatsuji, M. Caricato, X. Li, H. P. Hratchian, A. F. Izmaylov, J. Bloino, G. Zheng, J. L. Sonnenberg, M. Hada, M. Ehara, K. Toyota, R. Fukuda, J. Hasegawa, M. Ishida, T. Nakajima, Y. Honda, O. Kitao, H. Nakai, T. Vreven, J. A. Montgomery Jr., J. E. Peralta, F. Ogliaro, M. Bearpark, J. J. Heyd, E. Brothers, K. N. Kudin, V. N. Staroverov, R. Kobayashi, J. Normand, K. Raghavachari, A. Rendell, J. C. Burant, S. S. Iyengar, J. Tomasi, M. Cossi, N. Rega, J. M. Millam, M. Klene, J. E. Knox, J. B. Cross, V. Bakken, C. Adamo, J. Jaramillo, R. Gomperts, R. E. Stratmann, O. Yazyev, A. J. Austin, R. Cammi, C. Pomelli, J. W. Ochterski, R. L. Martin, K. Morokuma, V. G. Zakrzewski, G. A. Voth, P. Salvador, J. J. Dannenberg, S. Dapprich, A. D. Daniels, O. Farkas, J. B. Foresman, J. V. Ortiz, J. Cioslowski, D. J. Fox, *Gaussian16 (Revision C.01)*, Gaussian Inc. Wallingford CT, 2016.
- [47] G. H. F. Diercksen, B. O. Roos, A. J. Sadlej, *Chem. Phys.*, 1981, **59**, 29–39.
- [48] T. Lu, F. Chen, *J. Comput. Chem.*, 2012, **33**, 580–592.
- [49] I. Mayer, P. Salvador, *Chem. Phys. Lett.*, 2004, **383**, 368–375.
- [50] T. Lu, F. Chen, *J. Mol. Graph. Model.*, 2012, **38**, 314–323.
- [51] Z. Liu, T. Lu, Q. Chen, *Carbon*, 2021, **171**, 514–523.
- [52] J. Makowska, D. Uber, L. Chmurzyński, *J. Phys. Chem. B*, 2012, **116**, 653–659.
- [53] B. Barszcz, S. A. Hodorowicz, K. Stadnicka, A. Jabłońska-Wawrzycka, *Polyhedron*, 2005, **24**, 627–637.
- [54] B. Barszcz, S. Hodorowicz, A. Jabłońska-Wawrzycka, K. Stadnicka, *J. Coord. Chem.*, 2005, **58**, 203–208.
- [55] B. Müller, H. Vahrenkamp, *Eur. J. Inorg. Chem.*, 1999, 137–144.
- [56] B. Barszcz, T. Głowiak, J. Jezierska, *Polyhedron*, 1999, **18**, 3713–3721.
- [57] S. V. Kireev, S. L. Shnyrev, *Laser Phys.*, 2015, **25**, 075602.
- [58] P. P. Rosa, G. B. Laranjeira, L. R. V. Favarin, L. Pizzuti, A. M. Júnior, L.M.C. Pinto, C. C. Gatto, A. R. L. Caires, C. G. Oliveira, V. M. Deflon, G. A. Casagrande, *Inorg. Chim. Acta*, 2018, **483**, 293–298.
- [59] J. F. Ogilvie, W. R. Rodwell, R. H. Tipping, *J. Chem. Phys.*, 1980, **73**, 5221–5229.
- [60] M. Kowalik, J. Masternak, J. Brzeski, M. Daszkiewicz, B. Barszcz, *Polyhedron*, 2022, **219**, 115818.
- [61] E. C. Morais, G. G. Correa, R. Brambilla, P. R. Livotto, J. H. Z. dos Santos, M. B. Cardoso, *J. Sol-Gel. Sci. Technol.*, 2012, **64**, 324–334.
- [62] L. Liu, B. Su, Q. Wei, X. Ren, *Green Chem.*, 2021, **23**, 5866–5874.
- [63] K. Ye, Y. Yang, H. Chen, J. Wu, H. Wei, L. Dang, *Processes*, 2023, **11**, 2951.
- [64] Q. Jia, Y. Ni, Z. Liu, X. Gu, Z. Cui, M. Fan, Q. Zhu, Y. Wang, J. Ma, *J. Chem. Inf. Model.*, 2022, **62**, 4928–4936.
- [65] F. Wang, Y. Liu, H. Yan, D. Wang, Z. Chu, K. Li, L. Tong, M. Chen, J. Gong, *J. Mol. Liq.*, 2022, **366**, 120081.

